

Nanostructured Y-doped ZrO₂ powder: peculiarities of light emission under electron beam excitation

N. Korsunskaya¹, V. Papusha¹, O. Kolomyys¹, V. Strelchuk¹, A. Kuchuk¹, V. Kladko¹, Yu. Bacherikov¹, T. Konstantinova², and L. Khomenkova¹

¹ V. Lashkaryov Institute of Semiconductor Physics, 41 Pr. Nauky, 03028 Kyiv, Ukraine

² Donetsk Institute for Physics and Engineering named after O.O. Galkin of the NASU, 72 R. Luxemburg str., 83114 Donetsk, Ukraine

Received 29 September 2013, revised 11 February 2014, accepted 18 March 2014

Published online 30 April 2014

Keywords Y-doped ZrO₂, nanopowder, luminescence, XRD, TEM, Raman scattering

* Corresponding authors: e-mail kors@isp.kiev.ua, Phone: +38 044 5256340, Fax: +38 044 5258342; e-mail khomen@isp.kiev.ua, khomen@ukr.net, Phone: +38 044 5255775, Fax: +38 044 5258342

Present work deals with the study of luminescence and structural properties of Y-doped ZrO₂ nanopowders sintered by co-precipitation of Zr and Y nitrates. The structural and light emitting properties were controlled by X-ray diffraction, transmission electron microscopy, Raman scattering, photo- (PL) and cathodoluminescence (CL) methods. Generally, room temperature PL spectra showed several bands in UV-orange range, whose shapes depend on the excitation light wavelength. Along with this, CL spectra demonstrate additional “red” emission,

which intensity exceeds that of other CL bands. At lower temperatures, preferable enhancement of “red” CL band, its narrowing and peak position shift to the longer wavelengths were found. This behavior testifies to the non-elementary nature of “red” CL band. Its nature and mechanism of its excitation are discussed. It is supposed that some impurities (such as Fe and/or Zn) or complex defects, containing oxygen vacancies and these impurities, are responsible for “red” emission appeared under electron beam excitation only.

© 2014 WILEY-VCH Verlag GmbH & Co. KGaA, Weinheim

1 Introduction Luminescence emission is a subject of great interest not only from the basic point of view of materials science but for practical application as well. Luminescent materials can be used in fluorescent lamps, vacuum fluorescent display devices, color plasma display panels, electroluminescent flat panel displays, as scintillators for registration of high-energy radiation etc.

Zirconia (ZrO₂) has attracted considerable attention because of its mechanical, electric, thermal and luminescent properties. Emitting ZrO₂ allows the different application of this material, for example, for oxygen sensor [1, 2], laser techniques, biological labeling [3], thermoluminescent UV dosimeters etc. Besides broad-band emission offers also an application of zirconia for white light emitting devices [4].

Another important application is the detection of high energy radiation (X- and γ -rays, electron beam) that allows its using in scintillators as well as for visualization of high energy radiation. For instance, strong UV luminescence, peaked at 4.2 eV and ascribed to self-trapped excitons

(STE), was observed from ZrO₂ thin films with tetragonal structure at low temperature under excitation near the fundamental absorption edge (~5.8-6.0 eV) and above this [5]. Due to this fact, such material was proposed as promising scintillator [6]. However, STE emission is thermally quenched above 150 K but is still observed at 300 K. At the same time, pure and/or Y-stabilized ZrO₂ materials exhibit blue-orange radiative emission from defect states that dominates in the spectrum under band-to-band excitation at 300 K [7,8]. This visible emission is safe for human eyes and it is suitable for a visualization of high energy radiation.

One of the methods to investigate the radiative transitions in ZrO₂ materials is to study its emission under electron beam pumping, so called cathodoluminescence (CL), allowing easy realization of band-to-band excitation in wide band-gap materials. However, only a few works were devoted to CL investigation [9,10,11], but they demonstrated different CL bands. For example, in [10] two defect related bands were observed at 2.0-2.2 eV and 2.8-3.0 eV

and the higher-energy band was most efficient. At the same time, in [9] one PL band was detected at 2.5 eV. This can be due to different microstructure of ZrO₂ materials (type of crystalline lattice, size distribution of ZrO₂ grains and different nature of radiative defects) that depends on the fabrication approach. In particular, freestanding ZrO₂ nanocrystals with different sizes, studied in [12], exhibit the lowest CL intensity for the smallest size nanocrystals.

In the present work Y-doped ZrO₂ nanopowders were sintered by co-precipitation of Zr and Y nitrates. Their structural and light emitting properties were controlled by XRD and Raman scattering, photo- (PL) and cathodoluminescence (CL) methods. Broad luminescence spectra under both types of excitation were obtained at room temperature. It was found that among different defect-related bands, the red emission is most efficient and its nature is discussed.

2 Experimental details ZrO₂ nanopowders doped by different amount of Y₂O₃ (from 0 to 6 mol.%) were synthesized by a co-precipitation technique using ZrOCl₂·nH₂O and Y(NO₃)₃·nH₂O salts. The 25% NH₄OH water solution was used as precipitant. Sediments were mixed for 1 hour at room temperature at pH=9. After this, they were repeatedly washed, filtered with distilled water and then the hydrogel was dried in a microwave furnace and calcined at 700 °C for 2 hours. More details can be found elsewhere [13, 14].

Elemental analysis of different Y-doped ZrO₂ powders, abbreviated below as ZYO powders, was performed by means of X-ray fluorescent method using EXPERT 3L W144U setup. Relative mass contribution of single elements such as ⁸O, ³⁹Y and ⁴⁰Zr was detected and corresponding molar concentration was extracted. The increase of Y₂O₃ content from 0 up to 6.11 mol% was found following the variation of Y(NO₃)₃·nH₂O in initial salt mixture. Besides, the impurities ²⁶Fe and ³⁰Zn were detected also. Their content was about 0.33 mol% and 0.79 mol%, respectively.

The structural properties were investigated by means of the X-ray diffraction (XRD), micro-Raman (μ -RS) scattering and Transmission electron microscopy (TEM) methods. XRD data were collected in the range of $2\Theta=20-80^\circ$ using X'Pert Pro MPD diffractometer with CuK α wavelength ($\lambda=0.15418$ nm) with grazing geometry (the angle of incident beam was $\omega\sim 0.5^\circ$). TEM observation was performed with JEOL JEM 200A instrument. Nanopowders were dispersed by ultrasonic treatment at frequency 35 kHz and were plotted on carbon replica. More details can be found elsewhere [15].

The μ -RS spectra were detected using a Horiba Jobin T-64000 Raman spectrometer in 200-900 cm⁻¹ spectral range. A 325-nm line of He-Cd laser was used as the excitation source. The laser power was kept below 5 mW to prevent laser heating of sample investigated. In cathodoluminescence (CL) measurements the samples were excited by scanning electron beam in quasi-continuous re-

gime at accelerating voltage $E=75$ kV and current value $I=10-120$ μ A. Scan was formed as the standard TV raster of 2.4×1.8 cm² area with frequencies of X- and Y-sweep 15.625 kHz and 50 Hz respectively. For CL measurements ZrO₂ powder was placed on sapphire substrate. Luminescence light was detected in the direction of incidence of electron beam and passed through lead glass TF-7 window for X-ray protection.

Photoluminescence (PL) was excited by 267-nm light of Ti-sapphire laser or 325-nm line of He-Cd laser as well as by 514-nm and 647-nm lines of Ar⁺ laser. Luminescence light was dispersed by grating monochromator and registered by CCD camera (PL) or photomultiplier (CL). CL was detected in 380-800 nm spectral range at 300 K and 77 K, while PL was recorded in 280-860 nm interval at 300 K.

It is worth to note that the increase of Y₂O₃ content results in the increase of PL intensity. The powder with 6.11 mol.% of Y₂O₃ demonstrates most efficient emission. Thus, hereafter the results obtained for this ZYO powder will be described mainly.

3 Results

3.1 Structural properties and morphology The XRD pattern of ZYO powder shows several peaks and in the range $2\Theta=20-80^\circ$ (Fig. 1(a)). Most intense reflections were detected at $2\Theta\sim 30.3^\circ, 34.8^\circ, 35.4^\circ, 43.2^\circ, 50.5^\circ, 59.6^\circ, 60.1^\circ, 73.2^\circ$ and 74.3° . They correspond to different ZrO₂ crystallographic planes whose assignment to relevant crystalline phase (monoclinic, tetragonal or cubic) is based on the comparison with tabled XRD data. The detailed analysis of XRD peak positions showed that ZYO powder structure matches the reflections corresponded to tetragonal phase with following cell parameters: $a=b=0.361$ nm, $c=0.516$ nm, $\alpha=\beta=\gamma=90^\circ$ [16]. In fact, the presence of (111) peak at $2\Theta\sim 30.3^\circ$ is the evidence of the absence of monoclinic phase in our powders. Along with this, the peak at $2\Theta\sim 43.2^\circ$ (102) and the doublet at $2\Theta\sim 73.2^\circ$ (004) and 74.3° (400) are the features of tetragonal phase only (Fig. 1(a), insets). The 2Θ region containing (004) and (400) tetragonal doublets has been extensively used by researchers in order to distinguish the cubic from the tetragonal structure in zirconia [17, 18, 19] because XRD peak corresponding to single (400) reflection of cubic phase is at $2\Theta\sim 73.8^\circ$. Thus, one can conclude that the main phase presented in the powders with 6.11 mol % of Y₂O₃ is tetragonal phase.

Taking into account that the broadening of Bragg peaks is due to pure size effects, mean grain size, d , was directly deduced from the full width at half maximum (β_{hkl}) of the peaks. Using the classical Scherrer formula, $d_{hkl}=0.9\lambda/(\beta_{hkl}\cos\theta)$, it was found that $d\sim 13$ nm. This result was confirmed by TEM observation of the same powder (Fig. 1(b)).

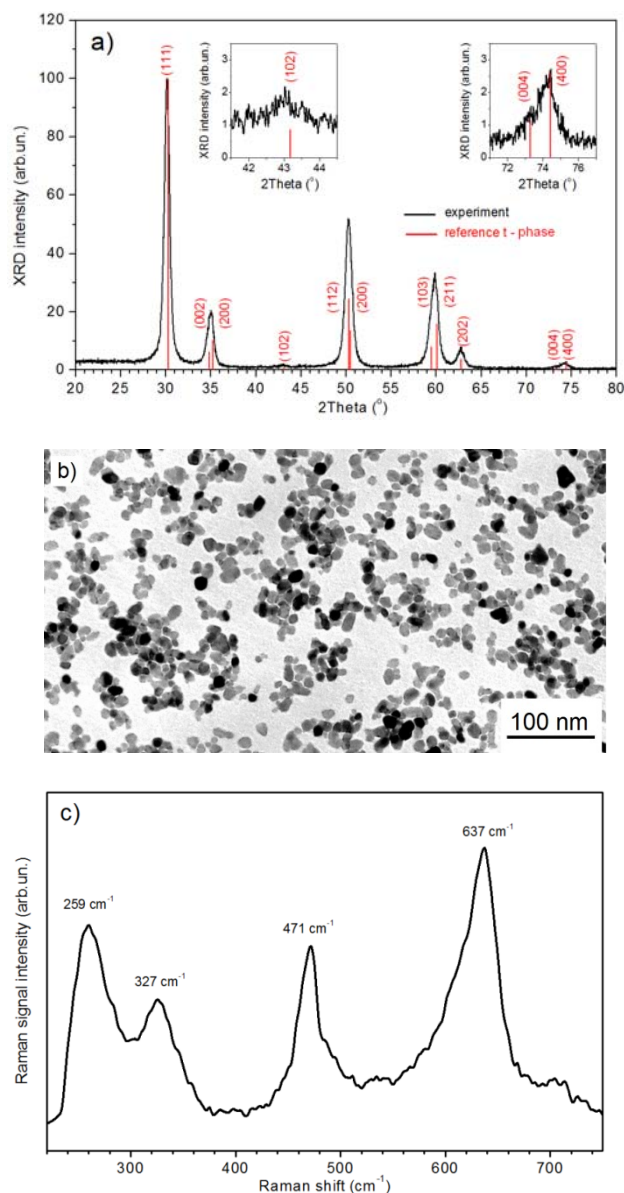


Figure 1 (a) X-ray diffraction pattern of ZYO powder. The insets demonstrate the peaks at $2\theta \sim 43^\circ$ and $\sim 74^\circ$ that are the features of tetragonal ZrO_2 phase only. Peak position and intensities of the reflexes of reference tetragonal phase (t-phase) are denoted as red bar [16]. (b) TEM bright field image and (c) UV Raman spectrum of the same powder.

The presence of tetragonal phase was revealed also by Raman scattering method. Figure 1(c) represents the UV Raman spectra of ZYO powder. Some broad bands peaked at 259, 327, 471, and 637 cm^{-1} are observed. The broad bands and low quality of the spectra could be due to structural distortion. The Raman bands at 259 and 327 cm^{-1} are exclusively assigned to the tetragonal phase of ZrO_2 [20]. The bands at 471 and 637 cm^{-1} are common for monoclinic or tetragonal phases, but their relative intensities are different for the two phases. For the tetragonal phase, the inten-

sities of these bands are about the same, or the magnitude of the band at 637 cm^{-1} is stronger, whereas in the case of monoclinic phase the intensity of the band at 471 cm^{-1} exceeds that of the band at 631 cm^{-1} [21]. On the other hand, both these bands are not detected for cubic phase and appear when this phase transforms to tetragonal one [22]. Thus, one can conclude that our samples contain mostly tetragonal phase.

3.2 Light emitting properties CL spectra of samples investigated at 300 K demonstrate two broad bands with maxima positions at 420 and 700 nm (blue and red bands) (Fig. 2). The intensity of red band exceeds essentially the intensity of blue one. The blue band has a long-wavelength tail that testifies to the presence of some other bands in blue-green spectral range. Such a band was often observed in PL, Roentgen luminescence and CL spectra [7, 10], but the red band at 700 nm, on our knowledge, was not earlier detected.

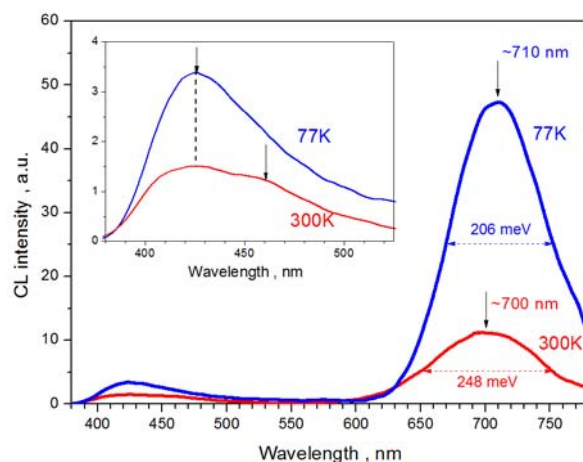


Figure 2 CL spectra of ZYO powders measured at 300 K and 77 K at $E = 75$ kV and $I = 120$ μA . The inset shows blue-green CL spectra in details.

The cooling to 77 K enhances the intensity of both bands but the red band increases mainly. Thus, the both bands show the thermal quenching in the range 77–300 K. Besides, the cooling results in the shift of red band peak position to low energy side and the decrease of its full width at half maximum (FWHM) (Fig. 2). Therefore, in spite of symmetric enough shape of red band we can conclude that it is also not elementary and with temperature decrease its low energy component increases mainly.

Figure 3 shows the dependencies of emission band intensities on electron beam current value where the results are plotted in log-log scale. This dependence for blue band can be approximated by a straight line in the whole used range of current values while the red band intensity reaches the saturation at $I > 55$ μA . The slopes of linear parts of these dependencies are lower than 1 and for blue band they increase with the increase of emission wavelength.

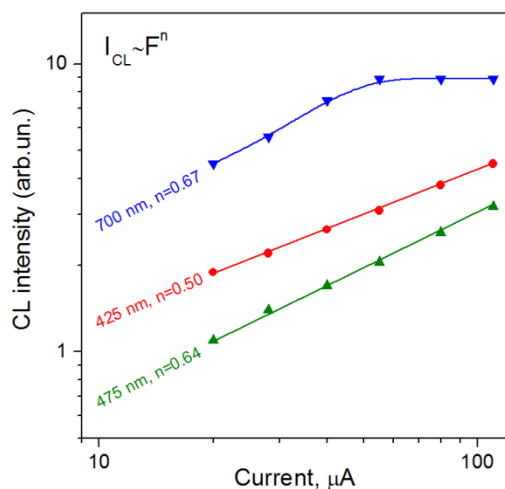


Figure 3 Variation of CL intensity versus electron beam current value for different CL bands.

In the case of band-to-band excitation that realized under electron beam irradiation (recombination luminescence) the sublinear ($n < 1$) dependence of emission intensity on intensity of excitation and subsequent saturation can be observed when the filling of emission centers by nonequilibrium carriers of one sign (minority carrier – carrier captured first) approaches to the center concentration [23]. Thus, we can suppose that this case is realized in our experiments. The saturation of blue band components at different I value can explain the dependence of n on registration wavelength observed for this band.

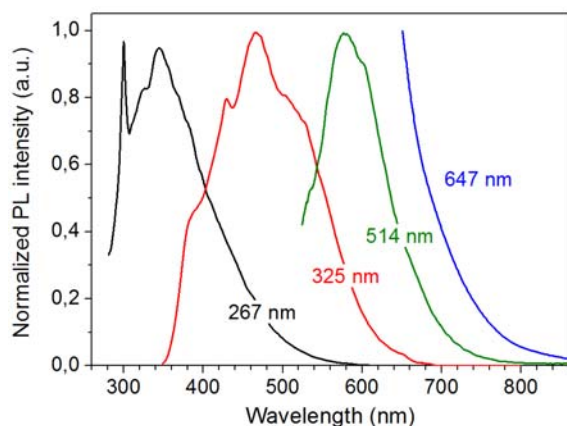


Figure 4 PL spectra of ZYO powder at different excitation wavelengths (mentioned in figure).

PL spectra recorded in 280–860 nm spectral range under excitation by the light of different wavelength are shown in Fig. 4. They demonstrate several overlapped defect-related bands besides the narrow peak at 290 nm caused obviously by self-trapped exciton [5]. The longer excitation wavelength in the range 267–514 nm, the longer wavelength of defect-related PL peak position was found.

Under $\lambda_{\text{exc}} = 647$ nm, only PL tail was observed. Thus, contrary to CL data, the red emission was not recorded under light excitation while blue band was clearly become apparent at $\lambda_{\text{exc}} = 325$ nm.

4 Discussion As it was mentioned above, both bands observed in CL shows the thermal quenching above 77 K. Unfortunately we could not measure the temperature dependence of CL intensity but the low temperature range of thermal quenching of these bands implies that activation energy (E_a) of quenching process cannot be high. Comparing with data of [4] we can suppose that it does not exceed 0.2–0.4 eV. The higher change of red band intensity with temperature in comparison with such a change of blue band means that activation energy of thermal quenching of this band exceeds the corresponding value for blue band. The same relationship takes place for low energy and high energy components of red band. Thus, the low energy CL band peak position the higher activation energy of thermal quenching that is in agreement of data of work [4].

The thermal quenching can be caused, in general, by two processes. One of them is the escape of one of the nonequilibrium carriers (generated in the emission center under electron beam excitation (delocalization of trapped charge carriers)) into permitted bands and its subsequent capture by nonradiative centers (external quenching). Figure 5(a) shows the different cases of external quenching for one- and two-level recombination centers. Another one is the competition between radiative and nonradiative electron transitions in the same center (intrinsic quenching). Activation energy, E_a , for external quenching is the distance between the energy level of emission center and nearest permitted band (Fig. 5(a, b)).

If the emission center introduces only one level in energy gap, the thermal quenching, depending on level position in band gap, can be caused by the thermal escape of carrier which is captured non-radiatively (Fig. 5(a)) or radiatively (Fig. 5(b)). In the first case, higher energy of CL band peak position will correspond to deeper level (i.e. lower E_a) and $E_a + E_{\text{CL}} \approx E_g$, where E_g is bandgap energy. This is usually observed in wide gap phosphors. In other case (Fig. 5(b)), the quenching energy is equal to emission quantum, i.e. $E_a \approx E_{\text{CL}}$.

If an internal quenching takes place, E_a is the barrier between minimum of potential curve (configuration-coordinate diagram) of excited state and intersection point of potential curves of excited and ground states (Fig. 5(c)). In this case the increase of E_a for low energy bands implies the decrease of the excited state curvature that accompanied by the decrease of their FWHM [4]. Unfortunately, all observed CL bands are non-elementary that makes a difficult an estimation of FWHM. Therefore, emission quenching mechanism needs further investigations. However, irrespectively of quenching mechanism, we can conclude that the recombination center responsible for red emission has, at least, two levels (excited and ground states) because

$E_a + E_{CL} < E_g$ and $E_a \neq E_{CL}$. Thus, red CL emission is most likely caused by intradefect transition (between excited and ground state of defect most likely) (Fig. 5(b, c)).

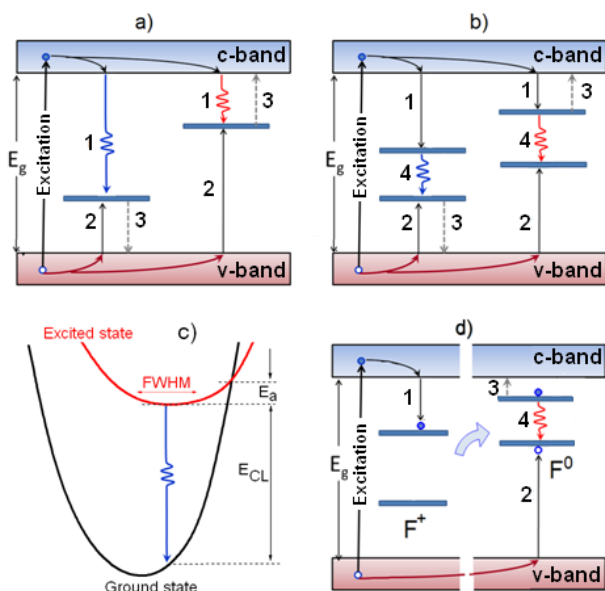


Figure 5 Simplified schemes of electron transitions in the case of one-level (a) and two levels' (b-d) radiative centers. The labels in the figures correspond to capture of free electrons (1) and free holes (2), thermal escape of electrons or holes (3), intradefect transition (4). Undulating arrows correspond to radiative transitions. (c) The coordination diagram showing the correspondence between emission energy (E_{CL}), FWHM and the activation energy of CL thermal quenching (E_a).

Radiative intradefect transition in visible range can be realized in some impurities as well as in the intrinsic defects (oxygen vacancies - F and F^+ centers or Zr^{3+}). But for wide luminescence band(s) in ZrO_2 the latter emission mechanism is currently generally accepted. Most of researchers attribute the different bands of ZrO_2 emission to oxygen vacancies in the volume of the crystallites/grains or located at their surface as well as near Y which stabilizes the tetragonal structure of ZrO_2 or near other defects (impurities, grain boundaries, etc.). This can explain the observation of the abundance of overlapped bands whose peak positions depend on crystallite size [7]. In particular, blue band with peak position 430-460 nm was attributed to intradefect transition in F^+ -centers while longer wavelength emission was ascribed to complexes including Y [4]. Based on the elemental analysis of our samples, one can supposed that the red emission is due to intradefect transition in Zn and/or Fe impurities. At the same time, it was observed the increase of its intensity with Y content, which stimulates the formation of oxygen vacancies [7]. Thus, one cannot exclude their role in red emission. It is probably that these vacancies are the part of the complexes containing Zn and/or Fe impurities.

In general case, for intradefect transitions (in the impurities or in oxygen vacancies) under band-to-band steady-state excitation, three types of the processes determine the recombination rate and, thus, the emission intensity and its saturation with pumping: (1) free electron capture by excited state of the center (Fig. 5(b), process 1); (2) radiative transition from excited to ground level of the center (Fig. 5(b), process 4); (3) the capture of non-equilibrium hole by ground state of the center (process 2). If the rate of the process 4 is lower than those of the processes 1 and 2, then the saturation of the CL intensity will be faster for the centers with lower rate of the transition 4 and, this center will be saturated at first, whereas the intensity in saturation regime will be determined by the number of the centers.

In opposite case (when process 4 is faster than processes 1 and 2), the saturation will be determined by carrier capture cross sections and the concentration of centers. If the process 1 is faster than process 2, then the concentration of electron locked on emitting centers approaches to centre concentration under pumping increase and results in the saturation of emission intensity [23].

If the oxygen vacancies are involved in the recombination process, one can suppose that under band-to-band excitation electron from c-band is captured quickly in the attractive field of positively charged F^+ -centers (Fig. 5(d), process 1), forming F^0 -center in excited state (Fig. 5(d)). Its relaxation to ground state (Fig. 5(d), process 4) can result in red emission. Thus, we attribute this emission to intradefect transition in F^0 -centers. Further hole capture results in the discharging of this F^0 -center and the formation of F^+ -center ready for the next radiative event.

The thermal quenching of red band can be caused by the external quenching (electron escape from excited state of F^0 -center (Fig. 5(d), process 3) or by hole escape from ground state of F^0 -center) and by internal quenching in F^0 -center (Fig. 5(c)).

After the electron capture, the hole from valence band is captured on neutral center (Fig. 5(d), process 2). It can also result in light emission because of low cross-section of such a centre for carrier capture and difficulties with energy relaxation for deep level. In this case the radiative hole recombination should be expected. In fact, this is usually observed in crystalline phosphors for band-to-level transition. However, we did not detect any emission bands correlated with the red one. One of the reasons can be the use lead glass window for X-ray protection that also absorbs UV light.

Let us analyze the dependence of both band intensities on electron beam pumping (Fig. 3). The interesting fact is that the intensity of red band exceeds essentially the intensity of blue one in spite of its intensity saturates at $I > 55 \mu A$. The higher red band intensity can be caused, in general, by higher center concentration, while its faster saturation can be due to lower relaxation time of carrier from excited to ground state of red centers (Fig. 5(b), process 4). On the other hand, if the rates of the process 1 and 2 are

lower than that of process 4 (Fig. 5(b)), such behavior of red band can be caused also by higher electron capture cross section by corresponding centers. In fact, the higher capture cross section results in rapid filling of the centers by electrons and can cause the faster saturation of luminescence [23].

As it was mentioned above, the red emission was not observed under optical excitation (267–647 nm in this study). It is possible that this light energy is outside of specific spectral range required for red band excitation. On the other hand, red PL emission can require the excitation quantum which energy is higher than ZrO₂ band gap. Because this PL band was observed under 75 keV electron beam excitation and its intensity exceeds the intensity of blue-green bands, it can be used for visualization of the radiation with quantum energy larger essentially than ZrO₂ band gap. However, it is worth to note that the energy of such radiation has to be below the threshold of defect generation.

5 Conclusion Y-doped ZrO₂ powder, obtained by sol-gel method, was investigated by XRD, TEM, Raman scattering, cathodo- and photoluminescence methods. The ZYO powder was found to be of tetragonal phase with grain sizes of about 13 nm. Cathodoluminescence spectra at 300 K demonstrate broad blue and red bands. The intensity of red CL band exceeds essentially that of blue one. The cooling to 77 K enhances the intensity of both bands, but the red emission increases mainly. Besides, the narrowing of the red band and its peak position shift to lower energy side confirm its non-elementary nature. This band is proposed to be originated from either intradefect transition in the impurities (Fe and/or Zn) or complexes such as “oxygen vacancy-impurity”. In the last case, red CL emission can be ascribed to radiative relaxation of electron from excited state to ground one inside F⁰-centers located near impurities (Fe, Zn) after trapping of free electrons by corresponding F⁺ center. The dominant contribution of red emission into CL spectra opens some perspectives for its application as a marker for high-energy radiation (with quantum energy higher than ZrO₂ band gap, but lower than the threshold of defect generation).

Acknowledgements This work is supported by the National Academy of Sciences of Ukraine (project III-4-11).

References

- [1] J. D. Fidelus et al., *Solid State Phenom.* **128**, 141 (2007).
- [2] J. D. Fidelus, W. Lojkowski, D. Millers, K. Smits, and L. Grigorjeva, *IEEE Sensors* **9**, 1268 (2009).
- [3] R. Jia, W. Yang, Y. Bai, and T. Li, *Opt. Mater.* **28**, 246 (2004).
- [4] N. G. Petrik, D. P. Taylor, and T. M. Orlando, *J. Appl. Phys.* **85**, 6770 (1999).
- [5] J. Robertson, *Eur. Phys. J. Appl. Phys.* **28**, 265 (2004).
- [6] M. Kirm, J. Aarik, and I. Sildos, *Nucl. Instrum. Methods Phys. Res. A* **537**, 251 (2005).
- [7] H. Nakajima and T. Mori, *J. Alloys Compd.* **408–412**, 728 (2006).
- [8] K. Smits, L. Grigorjeva, D. Millers, A. Sarakovskis, J. Grabis, and W. Lojkowski, *J. Lumin.* **131**, 2058 (2011).
- [9] M. Garcia-Hipolito, O. Alvarez-Fregoso, E. Martinez, C. Falcony, and M. A. Aguilar-Frutis, *Opt. Mater.* **20**, 113 (2002).
- [10] L. Grigorjeva, D. Millers, A. Kalinko, V. Pankratov, and K. Smits, *J. Eur. Ceram. Soc.* **29**, 255 (2009).
- [11] H. Ken Yueh, and B. Cox, *J. Nucl. Mater.* **323**, 57 (2003).
- [12] F. Ramos-Brito, M. Garcia-Hipolito, R. Martinez-Martinez, E. Martinez-Sanchez, and C. Falcony, *J. Phys. D, Appl. Phys.* **37**, L13 (2004).
- [13] T. Konstantinova, I. Danilenko, V. Glazunova, G. Volkova, and O. Gorban, *J. Nanopart. Res.* **13**, 4015 (2011).
- [14] T. Konstantinova, I. Danilenko, and V. Varyukhin *Springer Proc. Phys.* **146**, 135 (2013).
- [15] A. S. Doroshkevich, I. A. Danilenko, T. E. Konstantinova, G. K. Volkova, and V. A. Glazunova, *Crystallogr. Rep.* **55**, 863 (2010).
- [16] Powder Diffraction Files, Card No. 01-070-4427, Database Edition, International Centre for Diffraction Data (ICDD), Newton Square, PA 19073-3273, USA, 2005.
- [17] R. C. Garvie, R. H. Hannink, and R. T. Pascoe, *Nature* **258**, 703 (1975).
- [18] R. Srinivasan, R. J. De Angelis, G. Ice, and B. H. Davis, *J. Mater. Res.* **6**, 1288 (1991).
- [19] A. Benedetti, G. Fagherazzi, and F. Pinna, *J. Am. Ceram. Soc.* **72**, 467 (1989).
- [20] C. Li, and M. Li, *J. Raman Spectrosc.* **33**, 301 (2002).
- [21] L. Shi, K. C. Tin, and N. B. Wong, *J. Mater. Sci.* **34**, 3367 (1999).
- [22] K. Nomura, Y. Mizutani, M. Kawai, Y. Nakamura, and O. Yamamoto, *Solid State Ion.* **132**, 235 (2000).
- [23] V. E. Lashkarev, A. V. Lyubchenko, and M. K. Sheinkman, *Non-equilibrium processes in photoconductors - Neravnovesnye processy v fotoprovodnikakh* (Naukova dumka, Kyiv, 1981), p. 264.